Calibration of Sample-Time Error in a Two-Channel Time-Interleaved Analog-to-Digital Converter

Shafiq M. Jamal, *Member, IEEE*, Daihong Fu, Mahendra P. Singh, Paul J. Hurst, *Fellow, IEEE*, and Stephen H. Lewis, *Fellow, IEEE*

***Abstract*—Offset mismatch, gain mismatch, and sample-time error between time-interleaved channels limit the performance of time-interleaved analog-to-digital converters (ADCs). This paper focuses on the sample-time error. Techniques for correcting and detecting sample-time error in a two-channel ADC are described, and simulation results are presented.**

***Index Terms*—Calibration, time-interleaved analog-to-digital converter, timing error.**

I. Introduction

IN MIXED-SIGNAL systems with analog inputs, analog-to-digital conversion is a key function that enables digital processing of samples of the analog signal. The analog-to-digital converter (ADC) often limits the sampling rate of such a system. Time interleaving more than one ADC is a well-known technique that can be used to increase the maximum sample rate [1]–[16]. When each channel operates near the maximum speed that is possible in a given technology, time interleaving can potentially increase speed with smaller increases in area and power dissipation than without interleaving. Unfortunately, the performance of time-interleaved ADCs is sensitive to offset and gain mismatches as well as aperture errors between the interleaved channels. Much work has been done on calibration to correct for offset and gain mismatches [7], [10], [11], [15]. To avoid the problem of aperture errors, a single front-rank sample-and-hold amplifier (SHA) can be used in front of all the interleaved channels [2], [9]–[12], [15]. However, a front-rank SHA limits the overall speed and therefore the number of channels that can be interleaved in practice. Therefore, operating without a front-rank SHA and calibrating for the sample-time errors will increase the sampling rate.

Calibration of sample-time errors requires both detection and correction of timing errors. To detect sample-time errors in the foreground (when the ADC is not processing an input), a known sinusoidal input can be applied, and the sample-time errors can be extracted from the images in the output spectrum caused by sample-time errors using discrete Fourier transforms [4]. Another proposed method to measure the sample-time errors is to generate a ramp signal to the ADC input [13]. If the slope of the ramp is known, the sample time errors can be estimated from differences of the ADC outputs. This scheme requires generation of an accurate ramp signal. When used in the background, the ramp signal is added to the ADC input. Therefore, the ramp signal uses some of the input range of the ADC. Also, a frequency component at any multiple of the channel sample rate in the input signal will appear as a nonzero offset in each channel, and this offset will interfere with the proposed background measurement of sample-time errors.

Once the sample-time errors have been measured, there are two main options for correcting sample-time error. The sampling clock for each ADC could be adjusted to eliminate the sample-time error [4]. This approach requires some means of clock-edge control, which could increase the random jitter of each controlled clock. Alternatively, the sample-time error can be corrected by digitally processing the ADC outputs to interpolate the sample values that would have occurred at the ideal sample times [13], [16], [19], [20]. This second approach is attractive because it can be done with the required accuracy using digital signal-processing circuits, which are portable and will benefit from evolving scaled CMOS technologies.

The main contributions of this paper are the description and analysis of digital sample-time correction and detection of the sample-time error for two time-interleaved ADCs. The remainder of this paper is divided into six major sections. Section II reviews time-interleaved ADCs and their limitations. Section III gives the filters required to correct sample-time error. Section IV describes a method of detecting the timing error. Section V extends that detection to signals above the Nyquist frequency. Section VI presents simulation results.

II. Background

Fig. 1 shows a simplified block diagram of a two-channel time-interleaved ADC. It consists of two channels in parallel, an analog demultiplexer at the input and a digital multiplexer at the output. Each channel consists of an ADC that samples the input at half of the overall sampling rate f_s. During conversion, the analog demultiplexer selects each channel in a ping-pong manner to process the analog input signal. The corresponding digital multiplexer selects the digital output of the selected channel and forms an effectively high-speed ADC. With interleaving, the overall sampling rate is f_s. Although this structure increases the sampling rate by a factor of two, the overall performance of time-interleaved ADCs is sensitive to channel mismatch [1]–[16].

Manuscript received January 31, 2003; revised October 8, 2003. This was was supported by the University of California MICRO under Grant 01-050 and by the National Science Foundation under Grant CCR-99001925. This paper was recommended by Guest Editors A. Rodríguez-Vázquez, F. Mediero, and O. Feely.

S. M. Jamal and M. P. Singh were with the University of California, Davis, CA 95616 USA. They are now with Marvell Semiconductor, Sunnyvale, CA 94086 USA.

D. Fu was with the University of California, Davis, CA 95616 USA. She is now with Maxim Integrated Products, Sunnyvale, CA 94086 USA.

P. J. Hurst and S. H. Lewis are with the Solid-State Circuits Research Laboratory, Department of Electrical and Computer Engineering, University of California, Davis, CA 95616 USA. (e-mail: hurst@ece.ucdavis.edu).

Digital Object Identifier 10.1109/TCSI.2003.821302

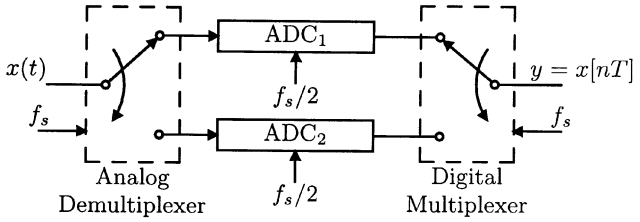

Fig. 1. Block diagram of the time-interleaved ADC architecture.

Different offsets in the ADC channels contribute to a dc value as well as a periodic additive pattern in the output of the ADC array. In the frequency domain, the periodic pattern appears as a tone at the channel sampling rate $f_s/2$, as is shown in the Appendix I.

Gain mismatches between the parallel channels cause amplitude modulation of the input samples by the sequence of channel gains. In the frequency domain, this error causes a copy of the input signal spectrum to appear centered around the channel sampling rate $f_s/2$. The expression for the ADC output with gain mismatch is derived in the Appendix II.

Ideally, each channel should sample T seconds after the previous channel, where $T = 1/f_s$. Deviations from the ideal sampling instants can be represented as a sequence of sample-time errors that introduce errors in the input samples. For a sinusoidal input, the input samples are phase modulated by the sequence of sample-time errors in the ADC channels. In the frequency domain, this error produces copies of the input signal spectrum at the same frequencies as the spurious components stemming from gain mismatch. Consider a two-channel ADC and assume that it is ideal except that there is a sample-time error. Let Δt be the deviation from the ideal sample time in the lower channel. Consider an input $x(t) = \cos(\omega_o t + \theta)$. (Throughout this paper, unless stated otherwise, the input frequency satisfies $0 < \omega_o < \omega_s/2$.) The ADC output is, as derived in Appendix III [see (45)]

$$y[n] = \underbrace{\cos\left[\frac{\omega_o \Delta t}{2}\right] \cos\left[\omega_o nT + \frac{\omega_o \Delta t}{2} + \theta\right]}_{\text{input}} + \underbrace{\sin\left[\frac{\omega_o \Delta t}{2}\right] \sin\left[\left(\omega_o - \frac{\omega_s}{2}\right) nT + \frac{\omega_o \Delta t}{2} + \theta\right]}_{\text{image}}. \quad (1)$$

In (1), the first term is the sampled input [scaled by $\cos(\omega_o \Delta t/2)$ and phase shifted by $\omega_o \Delta t/2$], and the second term is the image of the input due to sample time error. The image is frequency shifted by $\omega_s/2$ and phase shifted with respect to the input. If the sample-time error is small (i.e., $|\Delta t| \ll T$), then $\cos(\omega_o \Delta t/2) \approx 1$ and $\sin(\omega_o \Delta t/2) \approx \omega_o \Delta t/2$. Using these approximations, (1) can be written as

$$y[n] \approx \underbrace{\cos\left[\omega_o nT + \omega_o \frac{\Delta t}{2} + \theta\right]}_{\text{input}} - \underbrace{\frac{\omega_o \Delta t}{2} \sin\left[\left(\frac{\omega_s}{2} - \omega_o\right) nT - \omega_o \frac{\Delta t}{2} - \theta\right]}_{\text{image}}. \quad (2)$$

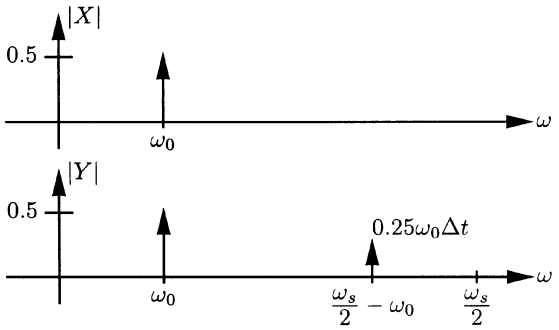

Fig. 2. Spectra of the input (X) and output (Y) in Fig. 1 with small sample-time error (Δt).

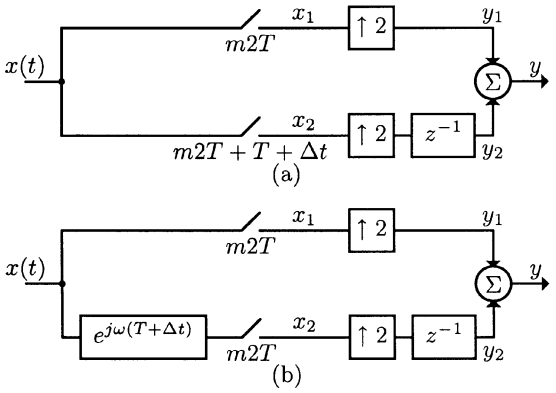

Fig. 3. (a) Block diagram of a two-channel time-interleaved ADC. (b) Model of (a).

This expression shows that the image amplitude is approximately proportional to the sample-time error Δt as well as the input frequency ω_o. Plots of the spectra of $y[n]$ and the input $x(t)$ are shown in Fig. 2.

All of these mismatches cause the noise floor of the ADC to increase, thus reducing the system signal-to-noise ratio (SNR) [1]–[16]. Techniques for correcting offset and gain mismatches have been presented elsewhere [10]–[12], [16]. The remainder of this paper will focus on methods of calibrating the sample-time error.

III. Sample-Time Error Correction

Fig. 3(a) shows a block diagram for a two-channel time-interleaved ADC. The input is $x(t) = \cos(\omega_o t + \theta)$. The top channel samples at times $m2T$, where m is a discrete time index. The lower channel samples the input at times $m2T + T + \Delta t$. Therefore, both channels sample at a rate $1/2T$, but the lower channel samples the input $T + \Delta t$ after the upper channel samples. Δt is the sample-time error for channel 2. Ideally, $\Delta t = 0$. The samples x_1 in the upper channel are upsampled by a factor of two to produce y_1. Similarly, the samples x_2 in the lower channel are upsampled by two and delayed to produce y_2. Signals y_1 and y_2 are then added to give the ADC output.

Fig. 3(b) shows an equivalent model of Fig. 3(a). Here the samplers in the two channels sample at the same times $m2T$, and the delay of $T + \Delta t$ associated with the sampling in the lower channel in Fig. 3(a) is modeled here by time-advancing the continuous-time input to the lower channel by $T + \Delta t$. The

$e^{j\omega(T+\Delta t)}$ block implements this time advance. Hence, the outputs of the corresponding samplers in Fig. 3(a) and (b) are identical. The samples x_1 and the upsampled signal y_1 are given by

$$x_1[m] = \cos[\omega_o(m2T) + \theta] \tag{3}$$
$$y_1[n] = \cos[\omega_o(nT) + \theta], \quad n = \text{even} \tag{4}$$
$$y_1[n] = 0, \quad n = \text{odd} \tag{5}$$

where m and n are discrete time indices. The signals in the lower channel are given by

$$x_2[m] = \cos[\omega_o(m2T + T) + \omega_o\Delta t + \theta] \tag{6}$$
$$y_2[n] = 0, \quad n = \text{even} \tag{7}$$
$$y_2[n] = \cos[\omega_o(nT + \Delta t) + \theta], \quad n = \text{odd}. \tag{8}$$

If the sample time error is zero ($\Delta t = 0$), the ADC output y becomes

$$y[n] = y_1[n] + y_2[n] = \cos(\omega_o nT + \theta). \tag{9}$$

Equation (9) shows that, in the ideal case ($\Delta t = 0$), the interleaved ADC output is samples of the input at a rate of $1/T$. With nonzero Δt, the output can be written as

$$y[n] = \cos\left\{\omega_o\left[nT + \frac{\Delta t}{2} - (-1)^n\frac{\Delta t}{2}\right] + \theta\right\}. \tag{10}$$

This equation shows that, with nonzero sample-time error, the interleaved ADC still samples the input at a rate of $1/T$; however, there is phase modulation due to the $(-1)^n\omega_o\Delta t/2$ term in (10). As described in Section II, this phase modulation contributes an undesired tone in the frequency domain. Equation (10) can be written as in (1) or more simply approximated by (2) under the assumption that the sample-time error is small. The frequency where the tone due to the sample-time error appears is called the image frequency and is equal to $\omega_i = \omega_s/2 - \omega_o$. The amplitude of the image is approximately proportional to both the sample-time error and the input frequency. In practice, minimizing the image amplitude is important to maximize the signal-to-noise-and-distortion ratio (SNDR) of the interleaved ADC.

If $\Delta t \neq 0$, the output y in Fig. 3 consists of samples of the input $x(t)$ taken at nonuniformly spaced sample times. If the continuous-time input $x(t)$ is bandlimited to less than $\omega_s/2 = \pi/T$, then the input $x(t)$ is nonuniformly sampled at an average sampling rate that satisfies the Nyquist criterion. Therefore, the continuous-time signal $x(t)$ can be reconstructed from x_1 and x_2 by appropriate filtering of the samples [21], [22] if Δt is known, and then the reconstructed output can be sampled at uniformly spaced sample times. Alternatively, the nonuniformly spaced samples can be converted to uniformly spaced samples by discrete-time filtering if Δt is known [13], [19], [20]. Such a system is shown in Fig. 4(a). The samples x_1 from the upper channel are upsampled by two and then filtered by $F_1(z)$. The samples x_2 from the lower channel are upsampled by two, then they are delayed by one sample. This delay assures that the upsampled signals are nonzero at different times, and this delay is the only processing that would be needed to generate the ADC output y without sample-time error. The upsampled and delayed signal is filtered by $F_2(z)$. Filters F_1 and F_2 together correct for sample-time error and give $y[n]$ that is uniformly spaced samples of the ADC input.

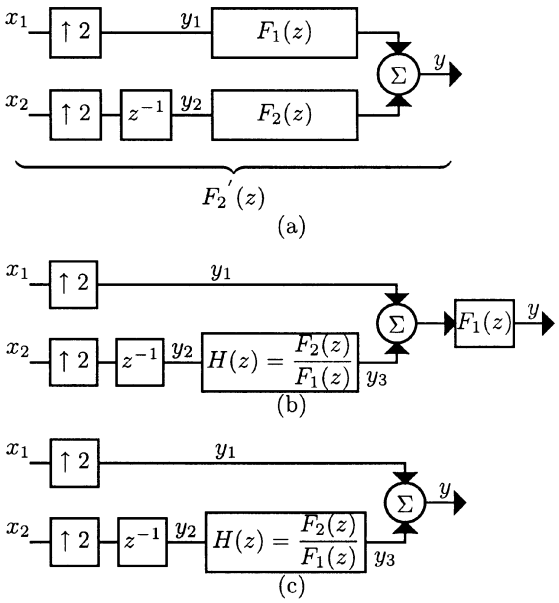

Fig. 4. (a) Processing required to correct for sample-time error. (b) Processing equivalent to the processing in (a). (c) The processing in (b) excluding the $F_1(z)$ filter.

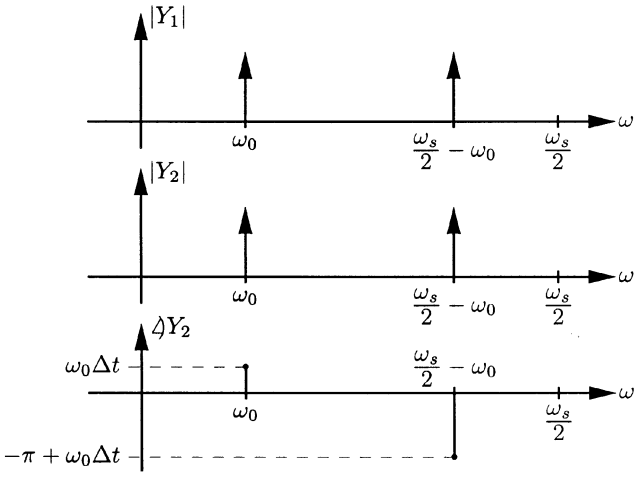

Fig. 5. Spectra of the signals y_1 and y_2 when $x(t) = \cos(\omega_o t)$.

For simplicity, consider an input signal $x(t) = \cos(\omega_o t)$. When sampled by the upper channel, the signal y_1 has the spectrum shown in Fig. 5. In this case, the spectrum is real (the phase is zero for every component). After the time-advance, sampling, and delay in the lower channel, the signal y_2 has the spectrum shown in Fig. 5. In this case, the phase of each component is nonzero. The goals of filters F_1 and F_2 in Fig. 4(a) are to eliminate the image components (at $\omega_s/2 - \omega_o$ and $-\omega_s/2 + \omega_o$) and to give an output y that is uniformly spaced samples of the continuous-time input.

To determine the filters that can generate uniformly spaced samples of the continuous-time input $x(t)$ from the nonuniformly spaced samples, consider an input signal $x(t) = \cos(\omega_o t + \theta)$. First, consider $e^{j\omega_o t + j\theta}$, the positive frequency component of the input $x(t)$. The processing in

Fig. 4(a) must give unity gain and zero phase shift at ω_o while eliminating the image component at $-\omega_s/2+\omega_o$, that is

$$F_1(\omega_o)+F_2'(\omega_o)e^{j\omega_o(T+\Delta t)} = 2 \quad (11)$$

$$F_1\left(\frac{-\omega_s}{2}+\omega_o\right)+F_2'\left(\frac{-\omega_s}{2}+\omega_o\right)e^{j\omega_o(T+\Delta t)} = 0. \quad (12)$$

Here, $F_2'(z)=F_2(z)z^{-1}$ has been used to simplify the equations. Second, consider $e^{-j\omega_o t-j\theta}$, the negative frequency component of the input $x(t)$. The processing in Fig. 4(a) must give unity gain and zero phase shift at $-\omega_o$ while eliminating the image component at $\omega_s/2-\omega_o$, that is

$$F_1(-\omega_o)+F_2'(-\omega_o)e^{-j\omega_o(T+\Delta t)} = 2 \quad (13)$$

$$F_1\left(\frac{\omega_s}{2}-\omega_o\right)+F_2'\left(\frac{\omega_s}{2}-\omega_o\right)e^{-j\omega_o(T+\Delta t)} = 0. \quad (14)$$

From the last four equations, F_1 and F_2 are given by

$$F_1(\omega)=\frac{e^{-j\frac{\pi\Delta t}{2T}\mathrm{sign}(\omega)}}{\cos\left(\frac{\pi\Delta t}{2T}\right)} \quad -\frac{\omega_s}{2}\le\omega\le\frac{\omega_s}{2} \quad (15)$$

and

$$F_2(\omega)=\frac{e^{-j\omega\Delta t}e^{j\frac{\pi\Delta t}{2T}\mathrm{sign}(\omega)}}{\cos\left(\frac{\pi\Delta t}{2T}\right)} \quad -\frac{\omega_s}{2}\le\omega\le\frac{\omega_s}{2}. \quad (16)$$

$F_1(\omega)$ and $F_2(\omega)$ are periodic with period ω_s because they are discrete-time filters. When $\Delta t=0$, $F_1(\omega)=1$ and $F_2(\omega)=1$, which is the signal processing shown in Fig. 3.

The filtering in Fig. 4(a) can be implemented as shown in Fig. 4(b), where F_1 now processes the summer output and $H(\omega)=F_2(\omega)/F_1(\omega)$ processes y_2. The expression for $H(\omega)$ is

$$H(\omega)=e^{-j\omega\Delta t}e^{j\frac{\pi\Delta t}{T}\mathrm{sign}(\omega)} \quad -\frac{\omega_s}{2}\le\omega\le\frac{\omega_s}{2}. \quad (17)$$

Fig. 4(b) still requires two separate filtering operations as in Fig. 4(a). A potential simplification is to eliminate F_1 from Fig. 4(b), as shown in Fig. 4(c). The images due to sample-time error are eliminated even if F_1 is deleted as in Fig. 4(c) because F_1 is an all-pass filter, so F_1 by itself cannot eliminate images. Although H is also an all-pass filter, it can eliminate images because it appears before the summer in Fig. 4(c). Therefore, the images have been eliminated in the summer output in Fig. 4(c). However, deleting F_1 introduces a small attenuation of $|\cos[\pi(\Delta t/2T)]|$ and a constant phase shift of $\pi(\Delta t/2T)$ in the final output. However, both of these effects are small in most practical cases. For example, if $|\Delta t/T|<1\%$, the resulting attenuation will be less than 1.1×10^{-3} dB and the phase shift will be less than 0.9 degrees. Therefore, one filter H as shown in Fig. 4(c) will suffice in many applications.

The filter H has a magnitude response of unity. Also, the negative of the slope of the phase response or the group delay of the filter is Δt except for discontinuities at kf_s, where k is any integer. This filter causes cancellation of the image generated by sampling time error for any input frequency between 0 and $f_s/2$. The impulse response corresponding to the frequency response $H(\omega)$ is

$$h[n]=-\frac{\sin\left(\pi\frac{\Delta t}{T}\right)}{\pi\left(n-\frac{\Delta t}{T}\right)}. \quad (18)$$

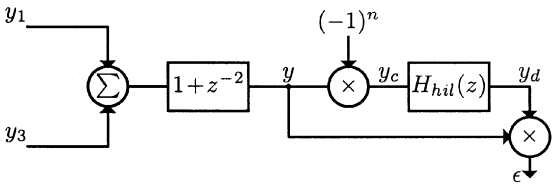

Fig. 6. Detection of the sample-time error. y_1 and y_3 come from Fig. 4.

This impulse response is infinite in extent. To make the filter causal and realizable in practice with a finite-impulse response (FIR) structure, the impulse response can be truncated, windowed, and delayed [17]. Any delay that is added to this filter must also be added to $y_1[n]$ in Fig. 4(c) before the summer to assure proper time alignment of the summed signals.

The filters described above can eliminate the effects of sample-time error if the sample-time error Δt is known. However, in most cases this sample-time error is unknown. Section IV describes a method to detect the sample-time error in the time-interleaved system.

IV. Sample-Time Error Detection

A. With Ideal Hilbert Filter

Fig. 6 shows the block diagram of a scheme that can detect the sample-time error using the input signal itself. The signals from the two channels are summed, and the summed output goes into a phase detector block. At the input of the detector, the signal is passed through a short FIR filter $(1+z^{-2})$. Ignore this filter at first. The output of the FIR filter is $y[n]$, which is chopped to produce $y_c[n]$; $y_c[n]$ is then passed through a Hilbert transform filter to produce $y_d[n]$. Then, $y[n]$ and $y_d[n]$ are multiplied. Assuming only a sample-time error of Δt, the ADC output with a sinusoidal input at ω_o is [from (45) in Appendix III]

$$y[n]=a\cos\left[\omega_o nT+\frac{\omega_o\Delta t}{2}+\theta\right] +b\sin\left[\left(\omega_o-\frac{\omega_s}{2}\right)nT+\frac{\omega_o\Delta t}{2}+\theta\right] \quad (19)$$

where $a=\cos(\omega_o\Delta t/2)$ and $b=\sin(\omega_o\Delta t/2)$ are constants. The chopped signal is

$$\begin{aligned} y_c[n] &= (-1)^n y[n] \\ &= a\cos\left[\left(\frac{\omega_s}{2}-\omega_o\right)nT-\frac{\omega_o\Delta t}{2}-\theta\right] \\ &\quad +b\sin\left[\omega_o nT+\frac{\omega_o\Delta t}{2}+\theta\right]. \end{aligned} \quad (20)$$

The chopped signal goes through an ideal discrete-time Hilbert transform filter [17], [18] to produce

$$y_d[n]=a\sin\left[\left(\frac{\omega_s}{2}-\omega_o\right)nT-\frac{\omega_o\Delta t}{2}-\theta\right] -b\cos\left[\omega_o nT+\frac{\omega_o\Delta t}{2}+\theta\right]. \quad (21)$$

Then y_d and y are multiplied. The product has a dc or average component that is equal to

$$\bar{\epsilon}=\overline{y_d\cdot y}=-ab=-\sin\left(\frac{\omega_o\Delta t}{2}\right)\cos\left(\frac{\omega_o\Delta t}{2}\right). \quad (22)$$

Assuming $|\omega_o \Delta t/2| \ll 1$, $\sin(\omega_o \Delta t/2) \approx \omega_o \Delta t/2$, and $\cos(\omega_o \Delta t/2) \approx 1$, (22) simplifies to

$$\bar{\epsilon} \approx -\frac{\omega_o \Delta t}{2}. \tag{23}$$

So $\bar{\epsilon}$ is approximately proportional to the sample-time error. Note that $|\bar{\epsilon}|$ increases with increasing input frequency, thus increasing the sensitivity of sample-time error detection with increasing input frequencies, where the image amplitude also increases.

This scheme for detecting sample-time error is based on the fact that the chopped image due to sample-time error is 90° out of phase with the input. Applying a Hilbert transform to the chopped signal eliminates the 90° phase difference between the frequency translated image and the input, causing $\bar{\epsilon} \neq 0$ when $\Delta t \neq 0$.

An ideal discrete-time Hilbert transform filter has transfer function $H_{\text{hil}}(\omega) = -j\text{sign}(\omega)$ for $-\omega_s/2 < \omega < \omega_s/2$, where sign() is the signum function. This filter has unity magnitude response and a constant phase shift of 90°. The impulse response of the Hilbert filter is [18]

$$h_{\text{hil}}[n] = \begin{cases} \dfrac{2}{\pi} \dfrac{\sin^2\left(\frac{\pi n}{2}\right)}{n}, & n \neq 0 \\ 0, & n = 0 \end{cases} \tag{24}$$

The discrete-time Hilbert filter in (24) is noncausal. To make the filter causal and realizable, the impulse response can be truncated, windowed, and delayed. The delay that is added to make the filter causal must also be added to $y[n]$ in Fig. 6 before it is multiplied by $y_d[n]$.

B. With Hilbert Filter Approximations

To accurately approximate the ideal discrete-time Hilbert transform filter, an FIR filter with a large number of taps is required, making it difficult to implement in practice. Simpler filters that approximate the Hilbert transform can be used instead of the discrete-time Hilbert filter for easier implementation. One simpler filter is a delay, or z^{-1} filter. This approximating filter can be used as $H_{\text{hil}}(z)$ in Fig. 6. This filter gives a constant magnitude response and linear phase shift. Using $H_{\text{hil}}(z) = z^{-1}$, the dc or average value of the product $\epsilon = yy_d$ is

$$\bar{\epsilon} = -ab\sin(\omega_o T) = -\cos\left(\frac{\omega_o \Delta t}{2}\right)\sin\left(\frac{\omega_o \Delta t}{2}\right)\sin(\omega_o T). \tag{25}$$

Assuming $|\omega_o \Delta t/2| \ll 1$, then

$$\bar{\epsilon} \approx -\frac{\omega_o \Delta t}{2}\sin(\omega_o T). \tag{26}$$

Note that the average value in (26) differs from that in (23) by a factor of $\sin(\omega_o T)$. The value in (26) is small for low input frequencies as in the Hilbert transform filter case; however, it does not monotonically increase with input frequencies as in the previous case. Here, $\bar{\epsilon}$ peaks when the input frequency is near $\omega_s/4$ and decreases to zero as the input frequency approaches $\omega_s/2$. Therefore, the sensitivity of the timing error detection decreases at high input frequencies where it is most important. Using a z^{-1} filter instead of the Hilbert transform filter has the advantage that it is easier to implement. However, since the phase shift of the z^{-1} filter is not a constant $-90°$, the output of the phase detector in Fig. 6 depends on timing error and gain mismatch (if gain mismatch exists), since the images due to gain and sample-time error appear at the same frequency and are 90° out of phase [cf. (40) and (45)]. Therefore, gain error must be corrected before the timing error can be corrected when using the z^{-1} approximation to the Hilbert filter.

Another simple approximation to the Hilbert transformer is a three-tap filter: $H_{\text{hil}}(z) = z^{-1} - z$. This filter gives the desired $-90°$ of phase shift at all frequencies, but its magnitude response is $2|\sin(\omega T)|$, which is not constant as desired. Using this filter for $H_{\text{hil}}(z)$ in Fig. 6, the dc or average value of the product $\epsilon = yy_d$ is

$$\bar{\epsilon} = -2ab\sin(\omega_o T) = -2\cos\left(\frac{\omega_o \Delta t}{2}\right)\sin\left(\frac{\omega_o \Delta t}{2}\right)\sin(\omega_o T). \tag{27}$$

Assuming $|\omega_o \Delta t/2| \ll 1$, then

$$\bar{\epsilon} \approx -\omega_o \Delta t \sin(\omega_o T). \tag{28}$$

Note that the average value in (28) differs from that in (23) and is twice the value in (26). An advantage of this three-tap approximation to the Hilbert transformer is that it gives the desired -90 degree phase shift for all frequencies, so the timing error detection is not affected by gain error (as is the case for the z^{-1} filter). In practice, a delay of one sample must be added to $H_{\text{hil}}(z)$ to make it causal, and $y[n]$ in Fig. 6 must be delayed by one sample before it is multiplied by $y_d[n]$.

C. Limitations

A problem with this detection technique occurs when the ADC input has a frequency component at $f_s/4$. In this case, the product of $y[n]$ and $y_d[n]$ may have a nonzero dc value even without timing error. [This occurs, for example, when $y[n] = \cos(n\pi/2 + \pi/4)$.] This dc value would indicate that a timing correction is needed even if no adjustment is necessary. To overcome this problem, the filter $1 + z^{-2}$ in Fig. 6 produces a null at $f_s/4$ to avoid the problem with inputs at this frequency (or inputs at frequencies that alias to $f_s/4$). Frequencies close to but not exactly equal to $f_s/4$ are attenuated somewhat by the $1 + z^{-2}$ filter. A sharper notch filter could be used in the detector if necessary.

Fig. 7 shows a feedback loop that includes timing error detection and correction. The detector output signal $\epsilon = y[n]y_d[n]$ is scaled by μ_t and becomes the input to an accumulator. In steady state, the average input to the accumulator must be zero. Therefore, the negative feedback loop drives $\bar{\epsilon}$ to zero. The filter $H(z)$ is a causal FIR approximation to (18), and the fixed delay in the upper channel equals the delay introduced in $H(z)$ to make it causal. The filter coefficients can be calculated, based on (18), or stored in a lookup table. In the steady state, the timing error is corrected and the images are eliminated as a result of finding and eliminating correlation between the sinusoidal input signal at frequency ω_o and the chopped and phase-shifted version of its image at $\omega_i = \omega_s/2 - \omega_o$. However, if the input signal $x(t)$ has frequency components at ω_o and ω_i with a nonzero phase difference between them, the average detector output ϵ will be nonzero even with no timing error,

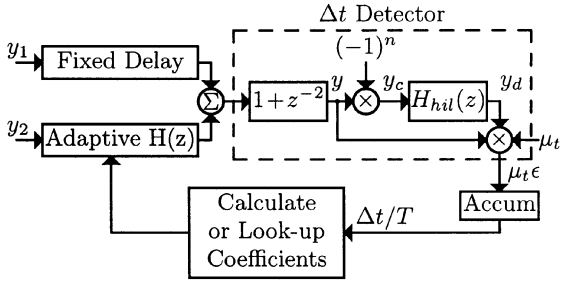

Fig. 7. Block diagram of the sample-time calibration approach.

which would cause the accumulator output and hence filter $H(z)$ to be incorrect. Therefore, one simple but restrictive condition for the timing-error detector to work properly is that the input signal $x(t)$ have a spectrum $X(\omega)$ that satisfies $|X(\omega)X(\omega_s/2-\omega)| = 0$. A less restrictive condition would be that the short-time Fourier transform $X_{\text{short}}(\omega)$ of the input signal [23] should satisfy $|X_{\text{short}}(\omega)X_{\text{short}}(\omega_s/2-\omega)| = 0$, for any short-time transform calculated over a time interval that is on the order of the time constant of the feedback loop in Fig. 7. If the input meets these conditions, the timing calibration can operate in the background on the input $x(t)$. If the input signal does not meet these conditions, then the proposed sample-time detection scheme could be used in the foreground with a test input that satisfies these conditions.

A FIR approximation to the sample-time correction filter cannot perfectly correct sample-time errors. Simulations show that a FIR filter has difficulty correcting sample-time errors for inputs near $\omega_s/2$ (see Section V). Therefore, the ADC input would have to be bandlimited to less than $\omega_s/2$ in practice. Assume that the input is bandlimited to $r\omega_s$, where $r < 1/2$. In this case, the condition $|X(\omega)X(\omega_s/2-\omega)| = 0$ will be satisfied for input frequencies $0 < \omega < (1/2-r)\omega_s$. Therefore, if the Δt detector in Fig. 7 is preceded by a filter that only passes signals in this frequency band and the corresponding image band $r\omega_s < \omega < \omega_s/2$, the sample-time calibration can operate in the background. A drawback of this approach is that the detection would be based on input frequencies near dc, which produce small images. In some cases, the spectrum of the input is zero in a frequency band near dc because the input is ac coupled or is a bandpass signal. In such a case, the condition $|X(\omega)X(\omega_s/2-\omega)| = 0$ will be satisfied for input frequencies near $\omega_s/2$. Then filtering before the detector to pass signals in this frequency band and its image band near dc allows the sample-time calibration to operate in the background. The advantage here is that the detection would be based on high-frequency inputs, which produce a larger detector output than low-frequency inputs.

V. Sample-Time Calibration for Input Frequencies Above $f_s/2$

The frequency responses of the digital filters H and F above are periodic with period f_s, but a sinusoidal input experiences a phase shift due to sample-time error that is periodic with period $1/\Delta t$. Therefore, the sample-time correction using $H(z)$ in (17) works only for input frequencies below $f_s/2$. However, operation for input frequencies above $f_s/2$ is possible by changing $H(z)$ to provide the proper phase shift to eliminate the resulting image. Operation for signals above $f_s/2$ may be of interest, for example, in a system that uses sampling in the ADC to mix a high-frequency bandpass signal to lower frequencies for processing. To eliminate the image due to sample-time errors for a sinusoidal input with frequency between $if_s/2$ and $(i+1)f_s/2$, equations equivalent to (11)–(14) can be solved for filters that keep the desired alias of the input signal while eliminating the undesired image. The resulting filter $H_i(z)$, which can replace $H(z)$ in Fig. 4(b) or (c) and eliminate the images due to sample-time error, is given by

$$H_i(\omega) = e^{-j\omega\Delta t}e^{jK\frac{\pi\Delta t}{T}\text{sign}(\omega)} \quad -\frac{\omega_s}{2} \le \omega \le \frac{\omega_s}{2} \tag{29}$$

where

$$K = \begin{cases} -i, & \text{if } i \text{ is odd} \\ i+1, & \text{if } i \text{ is even.} \end{cases} \tag{30}$$

The impulse response of this filter is

$$h_i[n] = \frac{\sin\left[(K-1)\pi\frac{\Delta t}{T} + n\pi\right] - \sin\left(K\pi\frac{\Delta t}{T}\right)}{\pi\left(n-\frac{\Delta t}{T}\right)}. \tag{31}$$

When $i = 0$ (and $K = 1$), the input frequency is less than $f_s/2$, and this equation gives $h_0[n]$ that is the same as $h[n]$ in (18).

Here, the filter F_1 in Fig. 4(b) is replaced by

$$F_{1,i}(\omega) = \frac{e^{-jK\frac{\pi\Delta t}{2T}\text{sign}(\omega)}}{\cos\left(K\frac{\pi\Delta t}{2T}\right)} \quad -\frac{\omega_s}{2} \le \omega \le \frac{\omega_s}{2} \tag{32}$$

where K is given in (30). Note that the phase error and attenuation that are being corrected by $F_{1,i}(\omega)$ increase as $|K|$ increases (i.e., as the input frequency moves to higher frequency bands).

The sample-time error detector in Fig. 6 can be used here because the aliased input and its image have the same relationship as when there is no aliasing, i.e., if the input frequency aliases to ω_o', the image appears at frequency $\omega_s/2 - \omega_o'$ and with a phase difference between them that is similar to the case when there is no aliasing. (See Appendix IV.) However, if the input frequency is between $if_s/2$ and $(i+1)f_s/2$ with i odd, the sign of the average detector output $\overline{\epsilon}$ changes from negative to positive, due to the different signs of the second terms in (47) and (49). Therefore, a negative value of μ_t is needed in Fig. 7 when i is odd to give negative feedback, while a positive value of μ_t is needed when i is even.

VI. Simulation Results

Simulations were carried out on the system in Fig. 7. Unless stated otherwise, simulations use a 29-tap FIR filter for $H(z)$ and a 21-tap FIR approximation for the Hilbert filter $H_{\text{hil}}(z)$ in Fig. 7, 10-b ADC quantization, sample-time error of $\Delta t/T = 0.01$, and $\mu = 2^{-23}$. The filter coefficients are found by multiplying the exact coefficients by a Hann window.

Fig. 8(a) shows the output spectrum of the ADC system with sample-time error. The input frequency is $f_o = 0.1f_s$. The image due to sample-time error appears at $f_i = 0.4f_s$. Fig. 8(b) shows the same output spectrum with sample-time correction after the loop in Fig. 7 has converged. The image amplitude has been reduced by about 40 dB and is small enough to give

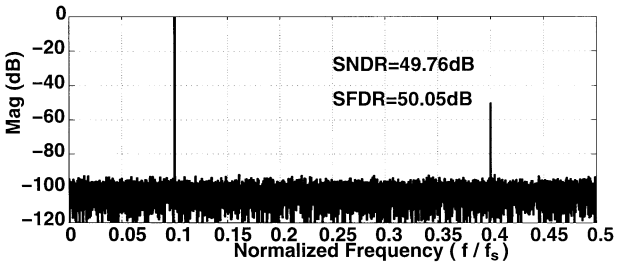

(a)

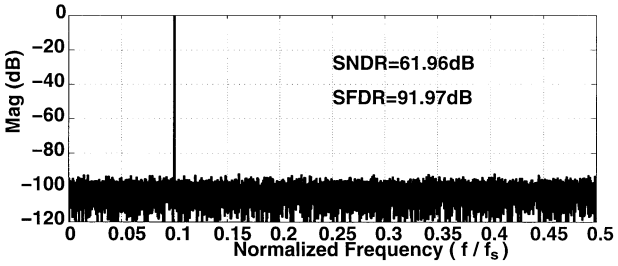

(b)

Fig. 8. The spectrum of the ADC output with sample-time error: (a) without and (b) with correction. $f_o = 0.1f_s$ and $\Delta t/T = 0.01$.

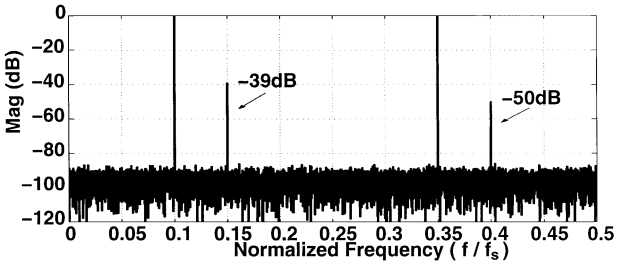

(a)

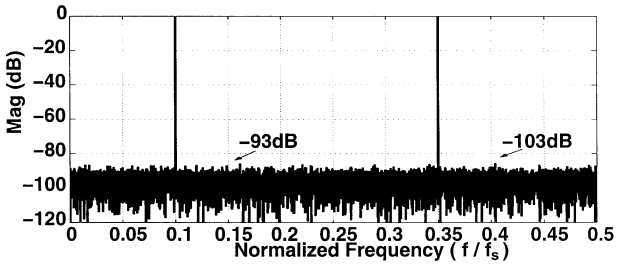

(b)

Fig. 9. ADC output spectra when the input consists of two equal-amplitude sinusoids at $0.1f_s$ and $0.35f_s$ and $\Delta t/T = 0.01$: (a) without and (b) with correction.

an SNDR of about 62 dB, which is expected for an ideal 10-b converter.

Fig. 9 shows spectra before and after sample-time correction when the input consists of two equal-amplitude sinusoids at $0.1f_s$ and $0.35f_s$. Here, there are two images caused by the two input frequencies, and their amplitudes are again much smaller after correction.

The accumulator output versus time is plotted in Fig. 10 for the sample-time correction system in Fig. 7. Two cases are plotted with $\Delta t/T = 0.02$ and $\mu_t = 2^{-12}$. The first uses

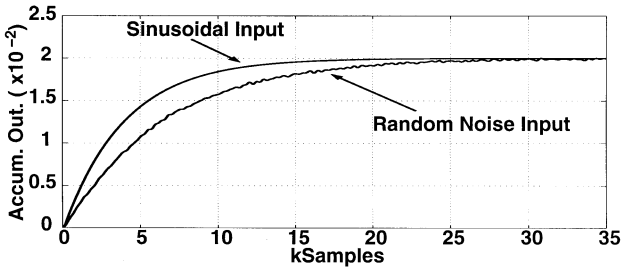

Fig. 10. Plots of the accumulator output versus time for the system in Fig. 7 using a 21-tap Hilbert filter for $H_{\rm hil}(z)$ with a sinusoidal input and with a white noise input. In both cases, $\Delta t/T = 0.02$ and $\mu_t = 2^{-12}$.

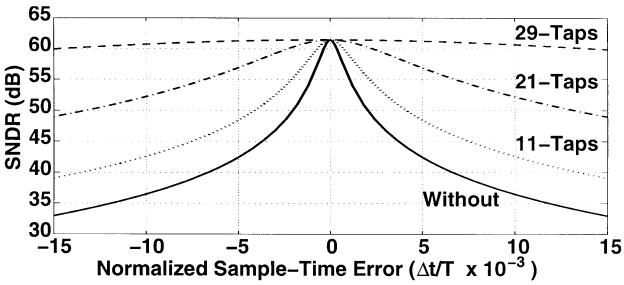

Fig. 11. Plots of SNDR versus sample-time error without and with calibration for different length FIR filters $H(z)$ with 10-b ADC quantization and a sinusoidal input at $f_o = 0.45f_s$.

TABLE I
FIR CORRECTION FILTER REQUIREMENTS FOR DIFFERENT ADC RESOLUTIONS

Number of ADC Bits	Number of Taps in $H(z)$	Number of Bits for Filter Coefficients
10	29	10
12	47	11
14	67	13
16	123	15

a sinusoidal input at $f_o = f_s/3$. The second uses a white noise input, bandlimited to $f_s/2$, with the same power as in the first case. In the steady state, negative feedback forces the average of the accumulator input to zero. Therefore, its output converges to $\Delta t/T = 0.02$ in both cases, which gives a $H(z)$ that corrects for the sample-time error.

Fig. 11 contains plots of SNDR versus timing error without and with calibration for different length FIR filters $H(z)$ for 10-b ADC quantization. The input is a sinusoid at $f_o = 0.45f_s$ or 90% of the Nyquist frequency. As the timing error increases, more taps are needed for correction.

Table I gives the number of filter taps needed in the FIR correction filter $H(z)$ in Fig. 7 for different ADC resolutions. The criterion used is that the corrected output should have a SNDR that is within 1 dB of the peak SNDR for $|\Delta t/T| < 1\%$. The input here is a sinusoid at $f_o = 0.45f_s$. The required length of the FIR correction filter increases with the number of bits in the ADC because more accuracy is needed in the filter to provide more attenuation of the image as the required SNDR increases. In practice, the filter coefficients must be quantized for a fixed-point implementation of the correction filter. The

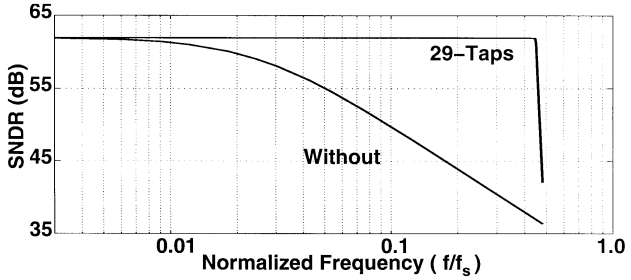

Fig. 12. Plots of SNDR versus input frequency for a sample-time error of $\Delta t/T = 0.01$ without and with calibration for 10-b ADC quantization. The input is a sinusoid.

number of bits required to keep the additional SNDR loss due to coefficient quantization to 0.1 dB is also given in Table I.

Fig. 12 shows plots of SNDR versus input frequency before and after calibration with a 29-tap FIR filter $H(z)$ for 10-b quantizers. This filter gives an SNDR $\geq$60 dB for input frequencies up to $0.45f_s$. The input is a sinusoid, and $\Delta t/T = 0.01$ in these simulations. Before calibration, as the input frequency increases, the SNDR drops monotonically because the effect of timing error is related to the slope of the input, which increases with the input frequency. Since the timing error increases with input frequency, more image attenuation is needed as the input frequency increases. To increase the image attenuation, more taps are needed to more accurately approximate the exact transfer function in (29).

VII. Conclusion

Techniques for detecting and correcting sample-time error in a two-channel ADC have been described. The detection and correction are implemented with digital signal processing. Such digital processing is attractive in scaled CMOS technologies. Correction is performed by digital filtering. The detector is based on the fact that if the ADC input contains a frequency component at ω_o, an image appears at $\omega_s/2 - \omega_o$. The image has an amplitude that is related to the sample-time error and, after chopping, the image is 90° out of phase with the input that caused it. The detection can be implemented in the background if the input signal satisfies conditions given in the paper. Otherwise, the detection can be implemented in the foreground using an appropriate input signal.

Appendix I
Offset Mismatch

A mathematical analysis of the output of a two-channel time-interleaved ADC with only offset error is given here. Assume channel one has offset $V_{\rm OS1}$, and channel two has offset $V_{\rm OS2}$. The output of the ADC in Fig. 1 with a sinusoidal input $x(t) = \cos(\omega_o t + \phi)$ is

$$y[n] = \cos(\omega_o nT + \phi) + V_{\rm OS1}, \quad n = \text{even} \tag{33}$$

$$y[n] = \cos(\omega_o nT + \phi) + V_{\rm OS2}, \quad n = \text{odd}. \tag{34}$$

Let $V_{\rm OS} = 0.5(V_{\rm OS1} + V_{\rm OS2})$ and $\Delta V_{\rm OS} = V_{\rm OS1} - V_{\rm OS2}$. Then the output can be written as

$$y[n] = \cos(\omega_o nT + \phi) + V_{\rm OS} + (-1)^n \frac{\Delta V_{\rm OS}}{2}. \tag{35}$$

Using $(-1)^n = \cos(\omega_s nT/2)$, (35) can be written as

$$y[n] = \cos(\omega_o nT + \phi) + V_{\rm OS} + \frac{\Delta V_{\rm OS}}{2} \cos\left[\left(\frac{\omega_s}{2}\right) nT\right]. \tag{36}$$

The second and third terms in (36) show that different offsets contribute to a dc value and a periodic additive pattern in the output of the ADC array.

Appendix II
Gain Mismatch

A mathematical analysis of the output of a two-channel time-interleaved ADC with only gain error is given here. Assume channel one has gain G_1, and channel two has gain G_2. Let $G = 0.5(G_1 + G_2)$ and $\Delta G = G_1 - G_2$. The ADC output with input $x(t) = \cos(\omega_o t + \phi)$ is

$$y[n] = \left[G + (-1)^n \frac{\Delta G}{2}\right] \cos(\omega_o nT + \phi). \tag{37}$$

Using trigonometric identities and $(-1)^n = \cos(\omega_s nT/2)$, (37) can be written as

$$y[n] = \left[G + \frac{\Delta G}{2} \cos\left(\frac{\omega_s nT}{2}\right)\right] \cos(\omega_o nT + \phi) \tag{38}$$

$$= G\cos(\omega_o nT + \phi) + \frac{\Delta G}{2} \cos\left(\frac{\omega_s nT}{2}\right) \cos(\omega_o nT + \phi) \tag{39}$$

$$= \underbrace{G\cos(\omega_o nT + \phi)}_{\text{input}} + \underbrace{\frac{\Delta G}{2} \cos\left[\left(\omega_o - \frac{\omega_s}{2}\right) nT + \phi\right]}_{\text{image}}. \tag{40}$$

In this equation, the first term is the scaled input and the second term is the image of the input due to channel gain mismatch. The last term in (40) shows that the image amplitude is proportional to the gain error ΔG.

Appendix III
Sample-Time Error

A mathematical analysis of the output of a two-channel time-interleaved ADC with only sample-time error is given here. Assume that the lower channel samples at a time $T + \Delta t$ after the upper channel, so there is a sample-time error in the lower channel of Δt. With the upper channel sampling at times $n2T$ and the lower channel sampling at times $n2T + T + \Delta t$, the combination of the two channels samples the input at times $nT + \Delta t/2 - (-1)^n \Delta t/2$. The ADC output with a sinusoidal input $x(t) = \cos(\omega_o t + \theta)$ is

$$y[n] = \cos(\omega_o t + \theta)|_{t = nT + \frac{\Delta t}{2} - (-1)^n \frac{\Delta t}{2}} \tag{41}$$

$$= \cos\left\{\omega_o \left[nT + \frac{\Delta t}{2} - (-1)^n \frac{\Delta t}{2}\right] + \theta\right\}. \tag{42}$$

Using $\cos(a-b)=\cos(a)\cos(b)+\sin(a)\sin(b)$ in the above equation gives

$$y[n]=\cos\left[\omega_o\left(nT+\frac{\Delta t}{2}\right)+\theta\right]\cos\left[(-1)^n\frac{\omega_o\Delta t}{2}\right]+\sin\left[\omega_o\left(nT+\frac{\Delta t}{2}\right)+\theta\right]\sin\left[(-1)^n\frac{\omega_o\Delta t}{2}\right]. \quad (43)$$

Using the facts that $cos()$ is even, $sin()$ is odd, and $(-1)^n=\cos(n\pi)$, (43) can be written as

$$y[n]=\cos\left[\omega_o\left(nT+\frac{\Delta t}{2}\right)+\theta\right]\cos\left[\frac{\omega_o\Delta t}{2}\right]+\sin\left[\omega_o\left(nT+\frac{\Delta t}{2}\right)+\theta\right]\cos(n\pi)\sin\left[\frac{\omega_o\Delta t}{2}\right]. \quad (44)$$

Using $\sin(a)\cos(n\pi)=\sin(a-n\pi)$ and $n\pi=\omega_s nT/2$ in the above equation gives

$$\begin{aligned}y[n]&=\cos\left[\frac{\omega_o\Delta t}{2}\right]\cos\left[\omega_o\left(nT+\frac{\Delta t}{2}\right)+\theta\right]+\sin\left[\frac{\omega_o\Delta t}{2}\right]\sin\left[\omega_o\left(nT+\frac{\Delta t}{2}\right)-\frac{\omega_s nT}{2}+\theta\right]\\&=\underbrace{\cos\left[\frac{\omega_o\Delta t}{2}\right]\cos\left[\omega_o nT+\frac{\omega_o\Delta t}{2}+\theta\right]}_{\text{input}}+\underbrace{\sin\left[\frac{\omega_o\Delta t}{2}\right]\sin\left[\left(\omega_o-\frac{\omega_s}{2}\right)nT+\frac{\omega_o\Delta t}{2}+\theta\right]}_{\text{image}} \quad (45)\end{aligned}$$

The image here is 90° out of phase with the image due to gain mismatch in (40). This can be seen by setting $\phi=\omega_o\Delta t/2+\theta$ in (40). The added phase shift of $\omega_o\Delta t/2$ stems from the average delay of $\Delta t/2$ caused by the sampling error of Δt in the lower ADC channel.

APPENDIX IV
SAMPLE-TIME ERROR FOR INPUT FREQUENCIES ABOVE $f_s/2$

An analysis of the output of a two-channel time-interleaved ADC with only sample-time error is given here, assuming a sinusoidal input with frequency greater than half the sampling frequency. In this case, aliasing occurs. If the input frequency is ω_o, it can be expressed as $\omega_o=\omega_o'+M\omega_s$, where M is a positive integer and $-\omega_s/2\le\omega_o'\le\omega_s/2$. With a sample-time error in the lower channel of Δt, the ADC output with a sinusoidal input at ω_o is given by (45), which is valid for any ω_o. Substituting $\omega_o'+M\omega_s$ for the second and fourth occurrences of ω_o in (45) gives

$$y[n]=\cos\left[\frac{\omega_o\Delta t}{2}\right]\cos\left[(\omega_o'+M\omega_s)nT+\frac{\omega_o\Delta t}{2}+\theta\right]+\sin\left[\frac{\omega_o\Delta t}{2}\right]\sin\left[\left(\omega_o'+M\omega_s-\frac{\omega_s}{2}\right)nT+\frac{\omega_o\Delta t}{2}\right)+\theta\Bigg]. \quad (46)$$

Using $M\omega_s nT=Mn2\pi$ and the periodicity of $sin()$ and $cos()$, (46) can be written as

$$y[n]=\underbrace{\cos\left[\frac{\omega_o\Delta t}{2}\right]\cos\left[\omega_o' nT+\frac{\omega_o\Delta t}{2}+\theta\right]}_{\text{aliased input}}+\underbrace{\sin\left[\frac{\omega_o\Delta t}{2}\right]\sin\left[\left(\omega_o'-\frac{\omega_s}{2}\right)nT+\frac{\omega_o\Delta t}{2}+\theta\right]}_{\text{image}}. \quad (47)$$

This equation is similar to (45). It shows that the aliased input and the image have the same phase and frequency relationships as when no aliasing occurs, as in (45).

If the sample-time error is small, then $\cos(\omega_o\Delta t/2)\approx 1$ and $\sin(\omega_o\Delta t/2)\approx\omega_o\Delta t/2$. Using these approximations, (47) can be written as

$$y[n]\approx\underbrace{\cos\left[\omega_o' nT+\frac{\omega_o\Delta t}{2}+\theta\right]}_{\text{aliased input}}-\underbrace{\frac{\omega_o\Delta t}{2}\sin\left[\left(\frac{\omega_s}{2}-\omega_o'\right)nT-\frac{\omega_o\Delta t}{2}-\theta\right]}_{\text{image}}. \quad (48)$$

This equation is similar to (2). It shows that the image amplitude is approximately proportional to the sample-time error Δt and the input frequency ω_o for small $|\Delta t|$.

The frequency ω_o' in (47) is negative if $i\omega_s/2<\omega_o<(i+1)\omega_s/2$ with i odd. To directly apply the analysis in Section IV to find the average detector output $\overline{\epsilon}$, an expression like (47) is needed where each frequency is positive and between 0 and $\omega_s/2$. Equation (47) satisfies this requirement for i even, as $\omega_o'>0$ in this case. For i odd, some manipulation allows (47) to be written as

$$y[n]=\underbrace{\cos\left[\frac{\omega_o\Delta t}{2}\right]\cos\left[|\omega_o'|\,nT-\frac{\omega_o\Delta t}{2}-\theta\right]}_{\text{aliased input}}-\underbrace{\sin\left[\frac{\omega_o\Delta t}{2}\right]\sin\left[\left(|\omega_o'|-\frac{\omega_s}{2}\right)nT-\frac{\omega_o\Delta t}{2}\right)-\theta\Bigg]}_{\text{image}}. \quad (49)$$

REFERENCES

[1] W. C. Black, Jr. and D. A. Hodges, "Time interleaved converter arrays," *IEEE J. Solid-State Circuits*, vol. SC-15, pp. 1022–1029, Dec. 1980.

[2] K. Poulton, J. J. Corcoran, and T. Hornak, "A 1-GHz 6-bit ADC system," *IEEE J. Solid-State Circuits*, vol. SC-22, pp. 962–970, Dec. 1987.

[3] Y. C. Jenq, "Digital spectra of nonuniformly sampled signals: fundamentals and high-speed waveform digitizers," *IEEE Trans. Instrum. Meas.*, vol. 37, pp. 245–251, June 1988.

[4] ——, "Digital spectra of nonuniformly sampled signals: a robust sampling time offset estimation algorithm for ultra high-speed waveform digitizers using interleaving," *IEEE Trans. Instrum. Meas.*, vol. 39, pp. 71–75, Feb. 1990.

[5] A. Petraglia and S. K. Mitra, "Analysis of mismatch effects among A/D converters in a time-interleaved waveform digitizer," *IEEE Trans. Instrum. Meas.*, vol. 40, pp. 831–835, Oct. 1991.

[6] M. Yotsuyanagi, T. Etoh, and K. Hirata, "A 10-b 50-MHz pipelined CMOS A/D converter with S/H," *IEEE J. Solid-State Circuits*, vol. 28, pp. 292–300, Mar. 1993.

[7] C. S. G. Conroy, D. W. Cline, and P. R. Gray, "An 8-b 85-MS/s parallel pipeline A/D converter in 1-μm CMOS," *IEEE J. Solid-State Circuits*, vol. 28, pp. 447–454, Apr. 1993.
[8] K. Nakamura, M. Hotta, L. R. Carley, and D. J. Allstot, "An 85 mW, 10 b, 40 Msample/s CMOS parallel-pipelined ADC," *IEEE J. Solid-State Circuits*, vol. 30, pp. 173–183, Mar. 1995.
[9] K. Y. Kim, N. Kusayanagi, and A. A. Abidi, "A 10-b, 100-MS/s CMOS A/D converter," *IEEE J. Solid-State Circuits*, vol. 32, pp. 302–311, Mar. 1997.
[10] K. C. Dyer, D. Fu, S. H. Lewis, and P. J. Hurst, "An analog background calibration technique for time-interleaved analog-to-digital converters," *IEEE J. Solid-State Circuits*, vol. 33, pp. 1912–1919, Dec. 1998.
[11] D. Fu, K. C. Dyer, S. H. Lewis, and P. J. Hurst, "A digital background calibration technique for time-interleaved analog-to-digital converters," *IEEE J. Solid-State Circuits*, vol. 33, pp. 1904–1911, Dec. 1998.
[12] K. C. Dyer, D. Fu, S. H. Lewis, and P. J. Hurst, "A comparison of monolithic background calibration in two time-interleaved analog-to-digital converters," in *Proc. IEEE Int. Symp. Circuits and Systems*, vol. 1, May 1998, pp. 13–16.
[13] H. Jin and E. K. F. Lee, "A digital-background calibration technique for minimizing timing-error effects in time-interleaved ADCs," *IEEE Trans. Circuits Syst. II*, vol. 47, pp. 603–613, July 2000.
[14] N. Kurosawa, H. Kobayashi, K. Maruyama, H. Sugawara, and K. Kobayashi, "Explicit analysis of channel mismatch effects in time-interleaved ADC systems," *IEEE Trans. Circuits Syst. I*, vol. 48, pp. 261–271, Mar. 2001.
[15] L. Sumanen, M. Waltari, and K. A. I. Halonen, "A 10-bit 200-MS/s CMOS parallel pipeline A/D converter," *IEEE J. Solid-State Circuits*, pp. 1048–1055, July 2001.
[16] S. M. Jamal, D. Fu, S. H. Lewis, and P. J. Hurst, "A 10-bit 120 Msample/s time-interleaved analog-to-digital converter with digital background calibration," *IEEE J. Solid-State Circuits*, vol. 37, pp. 1618–1627, Dec. 2002.
[17] A. V. Oppenheim and R. W. Schafer, *Discrete-Time Signal Processing*. Englewood Cliffs, NJ: Prentice-Hall, 1989.
[18] B. Porat, *A Course in Digital Signal Processing*. New York: Wiley, 1997.
[19] Y. C. Eldar and A. V. Oppenheim, "Filterbank reconstruction of bandlimited signals from nonuniform and generalized samples," *IEEE Trans. Signal Processing*, vol. 48, pp. 2864–2875, Oct. 2000.
[20] W. Namgoong, "Finite-length synthesis filters for nonuniformly time-interleaved analog-to-digital converter," in *Proc. IEEE Int. Symp. Circuits and Systems*, vol. 4, May 2002, pp. 815–818.
[21] J. L. Brown Jr., "Multi-channel sampling of low-pass signals," *IEEE Trans. Circuits Syst.*, vol. CAS-28, pp. 101–106, Feb. 1981.
[22] A. Papoulis, "Generalized sampling expansion," *IEEE Trans. Circuits Syst.*, vol. CAS-24, pp. 652–654, Nov. 1977.
[23] L. R. Rabiner and R. W. Schafer, *Digital Processing of Speech Signals*. Englewood Cliffs, NJ: Prentice-Hall, 1978.

Shafiq M. Jamal (S'94–M'01) was born in Kabul, Afghanistan, in 1974. He received the B.S., M.S., and Ph.D. degrees, all in electrical engineering, from the University of California, Davis, in 1996, 1999, and 2001, respectively.

Since July 2001, he has been with Marvell Semiconductor Inc., Sunnyvale, CA, working on high-speed data converters. His current research interests include mixed-signal circuit design in data communication and wireless communication.

Daihong Fu received the B.S. degree in electrical engineering from Tsinghua University, Beijing, China, in 1989, the M.S. degree in mathematics from Lamar University, Beaumont, TX, in 1992, and the M.S. and Ph.D. degrees in electrical engineering from the University of California, Davis, in 1996 and 1998, respectively.

She has been with Maxim Integrated Products, Sunnyvale, CA, since 1998. She has worked on the design of various analog ICs for audio, supervisory, and temperature sensors. Her research interests include analog and mixed-signal circuit design.

Mahendra P. Singh was born in Mysore, India, in 1979. He received the B.Tech degree in electrical engineering from Indian Institute of Technology, Delhi, in 2001 and the M.S. degree in electrical and computer engineering from the University of California, Davis, in 2002.

Currently he is working as a Design Engineer at Marvell Semiconductor, Sunnyvale, CA. His research interests include analog and mixed-signal design.

Paul J. Hurst (S'76–M'83–SM'94–F'01) received the B.S., M.S., and Ph.D. degrees in electrical engineering from the University of California, Berkeley, in 1977, 1979, and 1983, respectively.

From 1983 to 1984, he was with the University of California, Berkeley, as a Lecturer, teaching integrated-circuit design courses and working on an MOS delta-sigma modulator. In 1984, he joined the telecommunications design group of Silicon Systems Inc., Nevada City, CA, where he was involved in the design of CMOS integrated circuits for voice-band modems. Since 1986, he has been on the faculty of the Department of Electrical and Computer Engineering, University of California, Davis, where he is now a Professor. His research interests are in the areas of data converters and analog and mixed-signal integrated-circuit design for communication applications. He is a coauthor of the text book *Analysis and Design of Analog Integrated Circuits* (New York: Wiley, 2001, 4th ed.). He is also active as a consultant to industry.

Prof. Hurst was a member of the program committee for the Symposium on VLSI Circuits in 1994 and 1995, a member of the program committee for the International Solid-State Circuits Conference from 1998 until 2001, and a Guest Editor for the December 1999 issue of the IEEE JOURNAL OF SOLID-STATE CIRCUITS, for which he is now an Associate Editor.

Stephen H. Lewis (S'85–M'88–SM'97–F'01) received the B.S. degree from Rutgers University, New Brunswick, NJ, in 1979, the M.S. degree from Stanford University, Stanford, CA, in 1980, and the Ph.D. degree from the University of California, Berkeley, in 1987, all in electrical engineering.

From 1980 to 1982, he was with Bell Laboratories, Whippany, NJ. In 1988, he rejoined Bell Laboratories in Reading, PA. In 1991, he joined the Department of Electrical and Computer Engineering, University of California, Davis, where he is now a Professor. He is a coauthor of a college textbook on analog integrated circuits, and his research interests include data conversion, signal processing, and analog circuit design.

Dr. Lewis received the award for the Outstanding Engineering Scholar at Rutgers University, the Sakrison Memorial Prize at the University of California, Berkeley, and the IEEE Third Millennium Medal. Also, he was a co-recipient of the Jack Kilby Award for Outstanding Student Paper and the Beatrice Winner Award for Editorial Excellence at ISSCC. He was a member of the Program Committee for the International Solid-State Circuits Conference from 1994 to 1998, an Associate Editor of the IEEE JOURNAL OF SOLID-STATE CIRCUITS from 1994 to 1997, and Editor of the IEEE JOURNAL OF SOLID-STATE CIRCUITS from 1998 to 2001. He is now President of the IEEE Solid-State Circuits Society.